Journal of Molecular Liquids 299 (2020) 112133

Contents lists available at ScienceDirect

Journal of Molecular Liquids

journal homepage: www.elsevier.com/locate/molliq

Molecular dynamics simulation and theoretical study on heat capacities of supercritical H_2O/CO_2 mixtures

Xueming Yang [a,*], Yiyu Feng [a], Jianghao Jin [a], Yuanbin Liu [b], Bingyang Cao [b,*]

[a] Department of Power Engineering, North China Electric Power University, Baoding 071003, China
[b] Key Laboratory for Thermal Science and Power Engineering of Ministry of Education, Department of Engineering Mechanics, Tsinghua University, Beijing 100084, China

ARTICLE INFO

Article history:
Received 1 October 2019
Received in revised form 31 October 2019
Accepted 13 November 2019
Available online 25 November 2019

Keywords:
Heat capacity
Coal supercritical water gasification
Molecular dynamics simulation
Mixtures
Local structures

ABSTRACT

Molecular dynamics (MD) simulations and calculations based on the Peng-Robinson equation of state (PR-EOS) are carried out to compute the heat capacities of pure H_2O and CO_2 and supercritical H_2O/CO_2 mixtures. Using NIST data as a reference, it is found that the two methods generally exhibit comparable and acceptable performance in prediction of the heat capacities of the supercritical fluids. However, in near-critical region for pure supercritical H_2O and the supercritical H_2O/CO_2 mixtures at higher mole fractions of H_2O, PR-EOS exhibit poor prediction accuracy while MD simulation models achieve much better performance. The radial distribution function (RDF) and hydrogen bond analysis shows that this should contribute to the ability of MD simulations to deal with the effect of hydrogen bonding. This work is helpful for guiding the future investigation of the heat capacity of other working mixtures in thermodynamic systems based on the supercritical water gasification of coal.

1. Introduction

Coal is currently the most important fuel for thermal power generation in China due to its large storage capacity, wide distribution, and low price. The development of efficient and clean coal power generation technologies [1–4] is important for solving the problems of sustainable energy development and environmental pollution. In recent years, thermodynamic cycles based on working fluids of supercritical H_2O/CO_2 mixtures or supercritical CO_2 have received increasingly more attention. Guo et al. [1,2] proposed a thermodynamic cycle power generation system based on the supercritical water gasification of coal. This technology utilizes the particular physical and chemical properties of water in supercritical conditions, and converts the elements of hydrogen and carbon in coal into H_2 and CO_2. After combustion, the production of the supercritical H_2O/CO_2 mixtures can serve as the working fluids to flow into thermal power generation systems to generate electric power. Xu et al. [3,4] investigated a supercritical CO_2 (S-CO_2) coal-fired power plant and presented a 1000 MWe S-CO_2 coal-fired plant concept design. Compared with the previous supercritical water-steam Rankine cycle, the supercritical CO_2 Brayton cycle offers higher thermal efficiency, even when considering the post-combustion carbon capture process [5]. The supercritical fluids of pure CO_2 and H_2O/CO_2 mixtures offer desirable characteristics in clean coal power generation, and understanding their thermal properties, e.g., thermal conductivity, viscosity, PVT, and heat capacities, is the premise for the design and analysis of flow and heat transfer in thermal equipment [6–10]. Although there have been a few studies on the heat capacities of supercritical H_2O [11–14] and CO_2 [15–18], the research on the heat capacities of H_2O/CO_2 mixtures in supercritical regions of water remains limited, and the measurement is difficult.

The main simulation methods applicable to determine the thermophysical properties of fluids comprise molecular dynamics (MD) and Monte Carlo simulation (MC) [19]. MD simulation mainly relies on Newtonian mechanics to simulate the motion of the molecular system and obtain the structure and properties according to the motion state of the particles in the system. Endo et al. [20] used MD to obtain the heat capacity of silicon in different states at temperatures between 100 and 2500 K. The simulation results for amorphous silicon agree reasonably with those previous reported, and the heat capacity of amorphous silicon was found to be smaller than that of crystalline silicon at temperatures below 800 K but greater above 800 K. Nichele et al. [21,22] computed the heat capacity of Ar in the near-critical region and N_2 and O_2 along the $1P_c$ and $1.15P_c$ isobars in the temperature range from $0.8T_c$ to $1.2T_c$ by MD, and their results are in good agreement with the NIST data. Shvab et al. [23] used MD simulations with the rigid TIP4P/2005 and flexible TIP4P/2005f water models in the density range of 100–1000 kg/m^3 at a temperature of 670 K. Their results showed that the TIP4P/2005f potential cannot accurately reproduce the reference data, and the performance of TIP4P/2005 model is relatively well but it fails to predict the C_V minimum and C_P maximum.

* Corresponding authors.
E-mail addresses: xuemingyang@ncepu.edu.cn (X. Yang), caoby@tsinghua.edu.cn (B. Cao).

https://doi.org/10.1016/j.molliq.2019.112133
0167-7322/

Table 1
Force field parameters of the H_2O models used in this work.

		H_2O						
		SPC	SPC/E	SPC/Fw	TIP3P	TIP3P-ew	TIP4P	TIP4P/2005
ε (kcal/mol)	O-O	0.15535	0.15535	0.1554253	0.1521	0.102	0.155	0.1852
σ (Å)	O-O	3.166	3.166	3.165492	3.1506	3.188	3.15365	3.1589
q (e)	O	0.82	−0.8476	−0.82	−0.834	−0.83	−1.04	−1.1128
	H	0.41	0.4238	0.41	0.417	0.415	0.52	0.5564
r_O (Å)		1	1	1.012	0.9572	0.9572	0.9572	0.9572
θ_O (°)		109.47	109.47	113.240	104.52	104.52	104.52	104.52
r_{OM} (Å)	M	–	–	–	–	–	0.15	0.1546

MC method is mainly based on the random motion of particles in the system and combined with the probability distribution principle of statistical mechanics to obtain the thermodynamic properties of the system. Avendano et al. [19] used the MC method to calculate the isobaric heat capacity of CO_2 between 10 and 50 MPa, and an average absolute deviation of 2.71% was found between the results obtained with the SAFT-γ CG Mie model and the experimental results. Ishmael et al. [24] used MC simulations to calculate the C_P values of CO_2-methanol mixtures in the critical region. Simulated C_P values are generally in agreement with experimental values to within 3.5–5%, except for errors of up to 10–15% near the critical locus. Ghatee et al. [25] examined isochoric heat capacities of Hg and Cu by MC simulations, and their calcualtion values are in good agreement with experimental values.

The cubic equation of state (EOS) is also a commonly used method for predicting the thermodynamic properties of fluids. Congiunti et al. [26] compared different EOSs to determine the heat capacities of CO_2, H_2O, O_2, CH_4, and CO at temperatures between 100 and 1000 K and a pressure range from 50 to 300 bar. The comparisons show that the Peng-Robinson (PR) EOS is the best performer. Nasrifar et al. [27,28] used eleven state equations to calculate the thermodynamic properties of H_2. They found that all EOSs can well predict the heat capacities of hydrogen, and that the accuracies of the PT, RKS, and PR EOS were better. It is worth noting that the difference in $\alpha(T)$ functions in the EOS results in differences in the accuracy of prediction results. They also predicted thermodynamic properties of natural gas mixtures by using 10 EOSs, and the results show that the RKS and PR EOS with averages of absolute deviations of 1.34% and 1.43%, respectively, are slightly superior to the others in their ability to predict isobaric heat capacity.

In this work, MD simulation and PR-EOS are used to predict the heat capacities of pure H_2O, CO_2 and H_2O/CO_2 mixtures in supercritical regions of water, and the results obtained are compared to the National Institute of Standards and Technology (NIST) database [29].

2. Methodology

2.1. Force field and potential

When using MD simulation, selecting the appropriate potential and force field model is critical for predicting the heat capacity.

The total potential energy includes intramolecular and intermolecular terms ($U_{total} = U_{intramolecular} + U_{intermolecular}$). In this work, the combined Lennard-Jones (LJ) and Coulomb potential is adopted for intermolecular potential energy.

$$U_{\text{intermolecular}}(r_{ij}) = \begin{cases} 4\varepsilon_{ij}\left[\left(\frac{\sigma_{ij}}{r_{ij}}\right)^{12} - \left(\frac{\sigma_{ij}}{r_{ij}}\right)^{6}\right] + \frac{q_i q_j}{4\pi\varepsilon_o r_{ij}} & r_{ij} \le r_c \\ 0 & r_{ij} > r_c \end{cases} \quad (1)$$

In Eq. (1), r_{ij} is the distance between atoms i and j, r_c is the cutoff radius, ε_{ij} is the well depth, representing the interaction parameter of LJ potential between the two atoms, σ_{ij} is the core diameter, relating to the size parameter of LJ potential, q_i and q_j represent the electric charges of atoms i and j, respectively, and ε_0 is the vacuum permittivity.

Intramolecular energy terms to represent the bond and angle flexibility can be described by harmonic functions:

$$U_{\text{intramolecular}} = \frac{1}{2}k_r(r-r_0)^2 + \frac{1}{2}k_\theta(\theta-\theta_0)^2 \quad (2)$$

where r and r_0 represent the bond length at any time and equilibrium, respectively, θ and θ_0 represent the bending angle at any time and equilibrium, respectively, and k_r and k_θ are the bond stretching and angle bending energy constants, respectively.

With the detailed study of molecular models, many researchers have proposed a variety of H_2O and CO_2 force field models in recent years. Several common models are compared in this work, including the SPC model [30], SPC/E model [31], SPC/Fw model [32], TIP3P model [33], TIP3P-ew model [34], TIP4P model [33], and TIP4P/2005 model [35] for the study of pure H_2O. For the study of CO_2, the EPM model [36], EPM2 model [36], Cygan model [37], and TraPPE-flex model [38] are examined. The force field parameters of the models are listed in Tables 1 and 2. To describe the interaction between unlike atoms for pure fluid, the Lorentz-Berthelot (LB) combining rules is commonly adopted to determine the parameters of the LJ potential. It includes the Lorentz et al. [39] and Berthelot et al. [40] proposed geometric mean for ε_{ij} and arithmetic mean for σ_{ij}. Except for the EPM and EPM2 models of CO_2 [36], the characteristic distance σ_{ij} between different atoms has been given in the original literature by using the geometric mean rather than the arithmetic mean.

$$\begin{cases} \sigma_{ij} = \dfrac{\sigma_{ii} + \sigma_{jj}}{2} & \text{for } CO_2 \text{ of EPM, EPM2 model} \\ \sigma_{ij} = \sqrt{\sigma_{ii}\sigma_{jj}} & \text{otherwise} \end{cases} \quad (3)$$

$$\varepsilon_{ij} = \sqrt{\varepsilon_{ii}\varepsilon_{jj}} \quad (4)$$

In this work, three common combining rules for the H_2O/CO_2 mixtures are tested, including the LB rules, the Waldman-Hagler (WH)

Table 2
Force field parameters of the CO_2 models used in this work.

		CO_2			
		EPM	EPM2	Cygan	TraPPE-flex
ε (kcal/mol)	C-C	0.05760	0.05587	0.05593	0.05363
	O-O	0.16485	0.15991	0.15973	0.15691
σ (Å)	C-C	2.785	2.757	2.8	2.8
	O-O	3.064	3.033	3.028	3.05
q (e)	C	0.6645	0.6512	0.6512	0.7
	O	0.33225	0.3256	0.3256	0.35
r_O (Å)		1.161	1.149	1.162	1.16
θ_O (°)		180	180	180	180
k_r(kJ/mol·Å^2)		–	–	2017.925	2058.007
k_θ(kJ/mol·rad^2)		304.732	295.411	108.007	111.998

Table 3
Critical parameters and acentric factors of H_2O and CO_2.

	T_c(K)	P_c(MPa)	V_c(m^3/Kmol)	ω
H_2O	647.296	22.14020	0.05629781	0.343897
CO_2	304.169	7.378280	0.0942549	0.224877

rules [41] and Kong rules [42].

$$\begin{cases} \varepsilon_{ij}\sigma_{ij}^{\ 6} = \left(\varepsilon_{ii}\sigma_{ii}^{\ 6}\varepsilon_{jj}\sigma_{jj}^{\ 6}\right) \\ \frac{1}{2}\sigma_{ij} = \left(\frac{\sigma_{ii}^{\ 6}+\sigma_{jj}^{\ 6}}{2}\right)^{\frac{1}{6}} \end{cases} \text{WH rules} \tag{5}$$

$$\begin{cases} \varepsilon_{ij}\sigma_{ij}^{\ 6} = \left(\varepsilon_{ii}\sigma_{ii}^{\ 6}\varepsilon_{jj}\sigma_{jj}^{\ 6}\right) \\ \frac{1}{2}\varepsilon_{ij}\sigma_{ij}^{\ 12} = \frac{\varepsilon_{ii}\sigma_{jj}^{\ 12}}{2^{13}}\left[1+\left(1+\frac{\varepsilon_{jj}\sigma_{jj}^{\ 12}}{\varepsilon_{ii}\sigma_{ii}^{\ 12}}\right)\frac{1}{13}\right]^{13} \end{cases} \text{Kong rules} \tag{6}$$

2.2. Thermodynamic properties

The properties of isobaric heat capacity (C_P) and isochoric heat capacity (C_V) for pure H_2O and CO_2 fluids and H_2O/CO_2 mixtures are primarily studied in this work. In addition, the volume expansivity (α) and the isothermal compressibility (κ_T) are also calculated. Four thermodynamic properties are considered and evaluated via NPT ensemble fluctuation [43], and α and κ_T can be computed from the following expressions:

$$\alpha = \frac{\left\langle VH^{conf}\right\rangle - \langle V\rangle\left\langle H^{conf}\right\rangle}{\langle V\rangle k_B T^2} \tag{7}$$

$$\kappa_T = \frac{\left\langle V^2\right\rangle - \langle V\rangle^2}{\langle V\rangle k_B T} \tag{8}$$

where k_B is the Boltzmann constant, V is the system volume, p and T are the specified pressure and temperature, respectively, H_{conf} is the configurational enthalpy that can be computed from $H_{conf} = U_{conf} + pV$, and the angle brackets indicate ensemble averages.

For the calculation of the heat capacity, the isobaric heat capacity consists of two parts; $C_P = C_P^{id} + \Delta C_P$, where C_P^{id} is defined as the ideal contribution that can be taken individually from theory [44] and experimentally correlated [14,15] for H_2O and CO_2. The mixtures can be obtained by the formulation $C_P^{id} = \sum_{i=1}^{n} C_{P,i}^{id} x_i$. ΔC_P is the residual term that is mainly influenced by the intermolecular interaction:

$$\Delta C_P = \frac{\left\langle U^{conf}H^{conf}\right\rangle - \left\langle U^{conf}\right\rangle\left\langle H^{conf}\right\rangle}{k_B T^2} + p\frac{\left\langle VH^{conf}\right\rangle - \langle V\rangle\left\langle H^{conf}\right\rangle}{k_B T^2} - Nk_B \tag{9}$$

$$C_V = C_P - \frac{T\langle V\rangle\alpha^2}{\kappa_T} \tag{10}$$

where U_{conf} is the configurational internal energy, and N is the number of molecules used for the simulation.

For comparison with the simulation results, the Peng-Robinson cubic equation of state (PR-EOS) [45] is also used to compute the heat capacities, volume expansivity, and isothermal compressibility as follows.

$$p = \frac{RT}{v-b} - \frac{a}{v^2+2vb-b^2} \tag{11}$$

$$a(T) = a_c\alpha(T) \tag{12}$$

$$a_c = \frac{0.45724R^2T_c^{\ 2}}{p_c} \tag{13}$$

$$\alpha(T) = \left[1+(0.37464+1.54226\omega-0.26992\omega^2)\left(1-\sqrt{\frac{T}{T_C}}\right)\right]^2 \tag{14}$$

$$b = \frac{0.7780RT_c}{p_c} \tag{15}$$

$$C_P = C_P^{id} - R + T\left(\frac{\partial p}{\partial T}\right)_v\left(\frac{\partial v}{\partial T}\right)_p + T\int_{\infty}^{v}\left(\frac{\partial^2 p}{\partial T^2}\right)_v dv \tag{16}$$

$$C_V = C_V^{id} + T\int_{\infty}^{v}\left(\frac{\partial^2 p}{\partial T^2}\right)_v dv \tag{17}$$

$$\kappa_T = -\frac{1}{v}\left(\frac{\partial v}{\partial p}\right)_T \tag{18}$$

$$\alpha = \frac{1}{v}\left(\frac{\partial v}{\partial T}\right)_p \tag{19}$$

In Eqs. (11)–(19), C_V^{id} is the ideal isochoric heat capacity, and can be calculated by $C_V^{id} = C_P^{id} - R$. Additionally, R is the gas constant (R = 8.314472 J/(mol · K), p is the pressure, T is the temperature, a_c and b are EOS constants, v is the molar volume, T_c, P_c, V_c are the critical

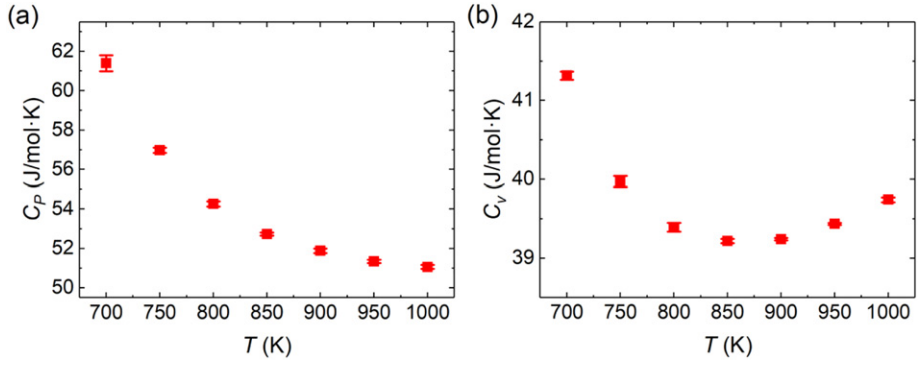

Fig. 1. Heat capacities calculated by MD simulation for H_2O/CO_2 mixtures (x_{CO_2} = 40%) with different system size. (a) isobaric heat capacity; (b) isochoric heat capacity.

temperature, pressure, and volume, respectively, and ω is the acentric factor. The relevant critical parameters of H_2O and CO_2 are listed in Table 3.

In the calculation of binary mixtures, the parameters a_m and b_m are obtained from the parameters of each pure component via the van der Waals mixing rule [46]:

$$a_m = \sum_i \sum_j x_i x_j a_{ij} \tag{20}$$

$$a_{ij} = (1-k_{ij})\sqrt{a_i a_j} \tag{21}$$

$$b_m = \sum_i x_i b_i \tag{22}$$

where x_i and x_j are the mole fractions of the mixture components i and j, respectively, and k_{ij} is called the binary interaction parameter, which is important for computing the thermodynamic properties of mixtures when using cubic EOS. In this work, the value of k_{ij} is based on the critical volume of pure fluid according to the study by Poling et al. [47].

$$k_{ij} = 1-8\frac{\sqrt{V_{c,i}\times V_{c,j}}}{\left(\sqrt[3]{V_{c,i}}+\sqrt[3]{V_{c,j}}\right)^3} \tag{23}$$

2.3. Simulation detail

All MD simulations are performed in NPT ensemble using the LAMMPS package [48], and conducted in a three-dimensional cube box with periodic boundary conditions in the X, Y, and Z directions. The equation of motion is integrated with the velocity Verlet algorithm [49] using a time step of 1.0 fs. The standard particle-particle-particle mesh (PPPM) method is used in long-range interactions with a cutoff distance of 13Å and a relative error in forces of 1×10^{-4}. The Nose-Hoover thermostat and barostat method are used in the NPT ensemble to control the temperature and pressure in the simulation. The total simulation time is 10 ns; the first 5 ns is the equilibration period, and the following 5 ns are performed to calculate the ensemble averages, during which the thermodynamics information is recorded every 1 ps.

3. Results and discussion

The effect of the system size on the heat capacity for the MD simulation must be examined. A series of simulations is carried out using the TIP4P model and TraPPE-flex model for H_2O/CO_2 mixtures (x_{CO_2} = 40%) with a molecular number of N = 1000–5000 at a pressure of 25 MPa. The simulation results are presented in Fig. 1. The heat capacities calculated with different numbers of molecules are basically in agreement with each other, i.e., the heat capacity is insensitive to system size. Considering the computational cost and the accuracy of the simulation results, N = 1000 is used to perform all the subsequent simulations.

3.1. Pure H_2O and CO_2

First, the heat capacity and relevant thermodynamic properties of pure H_2O at 25 MPa in the temperature range from 700 to 1000 K are

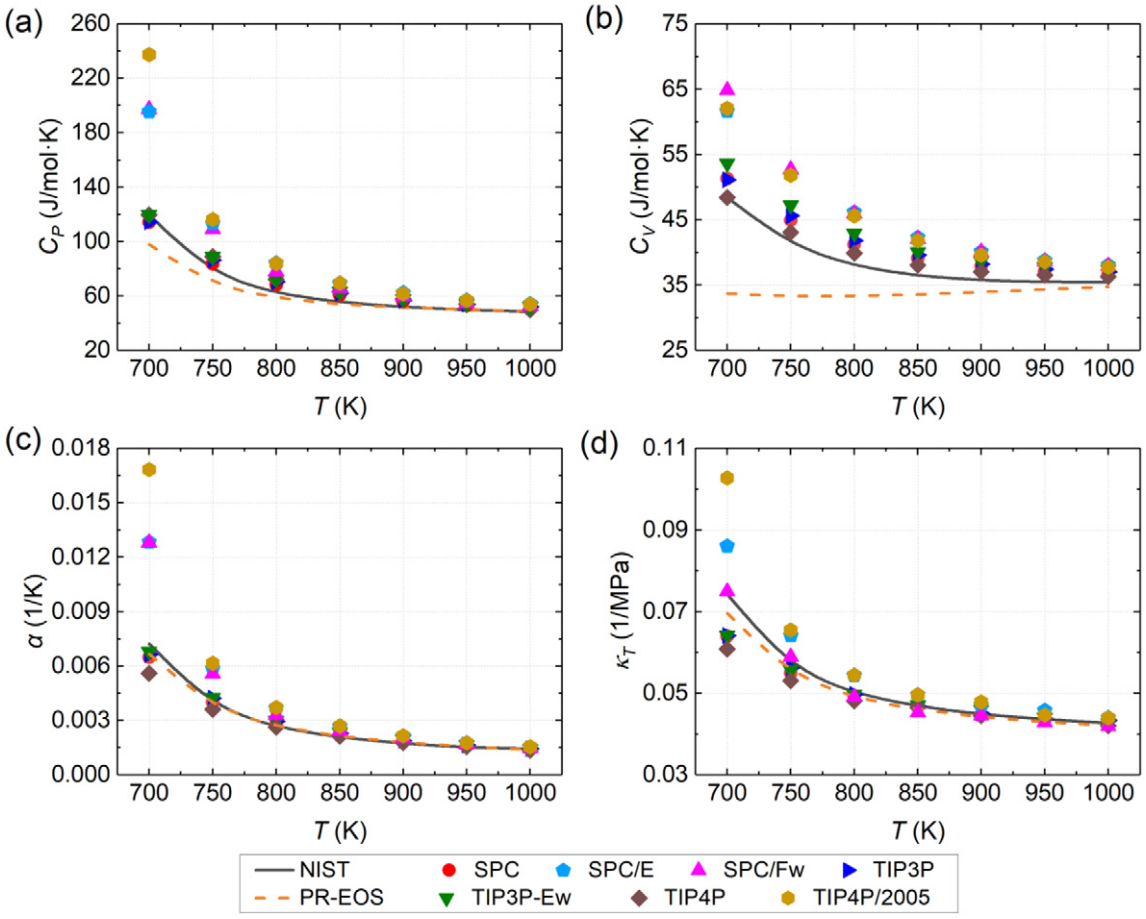

Fig. 2. The calculated thermophysical properties of H_2O by MD simulations with different H_2O force field models and PR-EOS and compared with NIST data. (a) isobaric heat capacity; (b) isochoric heat capacity; (c) volume expansivity; (d) isothermal compressibility.

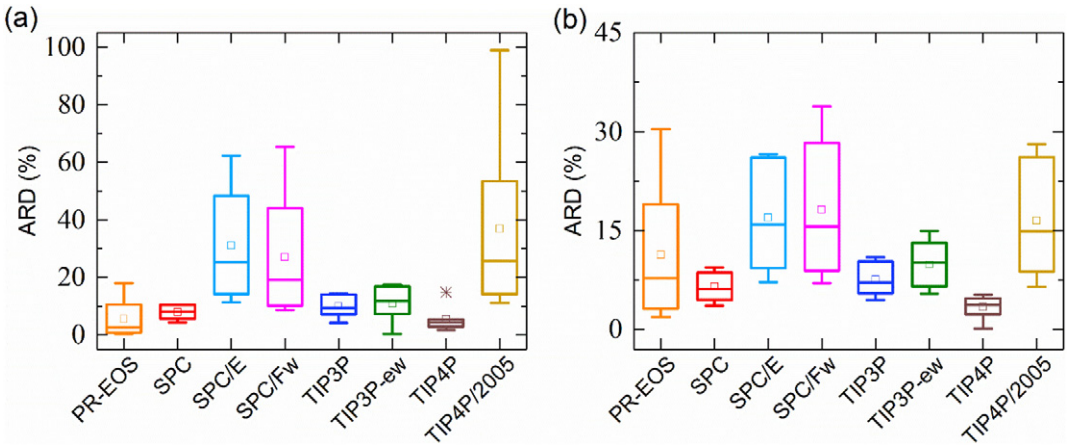

Fig. 3. ARDs of the calculated heat capacities for H_2O by MD simulations with different force field models and PR-EOS. (a) isobaric heat capacity; (b) isochoric heat capacity.

calculated using MD simulations and compared to the results predicted by PR-EOS. MD simulations are conducted using seven common force fields of pure H_2O, including SPC, SPC/E, SPC/Fw, TIP3P, TIP3P-ew, TIP4P, and TIP4P/2005. The thermodynamic properties C_P, C_V, α, and κ_T are obtained by the fluctuation theory and calculation formula (Eqs. (7)–(10)). As shown in Fig. 2, it was found that the four studied thermodynamic properties exhibit the same trend; they decrease with the increase of temperature. In addition, the SPC/E, SPC/Fw, and TIP4P/2005 models significantly overestimate these thermodynamic properties at a temperature of 700 K, and the PR-EOS calculations are inaccurate for predicting the trend of isochoric heat capacity. To clarify the comparison and discussion, the absolute relative deviation (ARD) between the MD simulation (or PR-EOS) results and the NIST data are calculated as:

$$ARD = \left|\frac{A^{CALC} - A^{NIST}}{A^{NIST}}\right| \times 100\% \tag{24}$$

where A^{CALC} is the predicted result from either the MD simulation or PR-EOS, and A^{NIST} denotes the reference data from NIST.

As is evident from Fig. 3, the deviations of the C_P, C_V, and α values of the TIP4P model are the smallest for pure water, with average ARDs (AARDs) of 5.38%, 3.40%, and 5.31%, respectively. Additionally, the κ_T

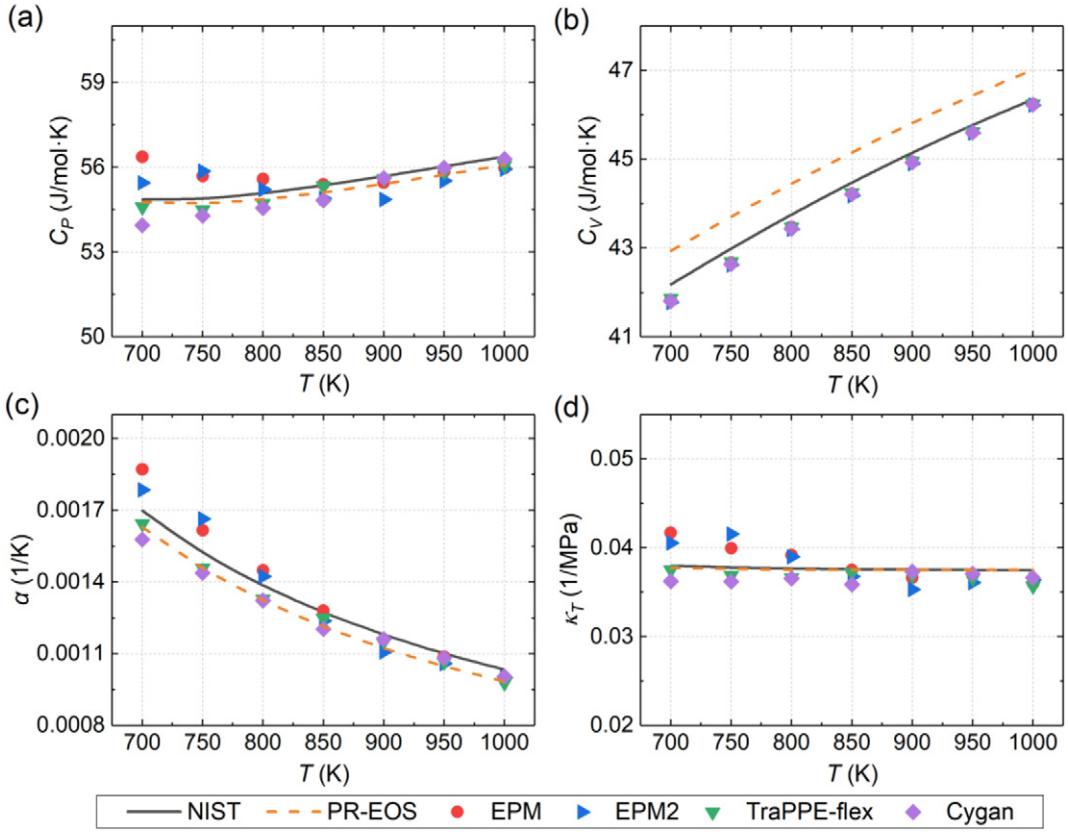

Fig. 4. The calculated thermophysical properties of CO_2 by MD simulations with different CO_2 force field models and PR-EOS and compared with NIST data. (a) isobaric heat capacity; (b) isochoric heat capacity; (c) volume expansivity; (d) isothermal compressibility.

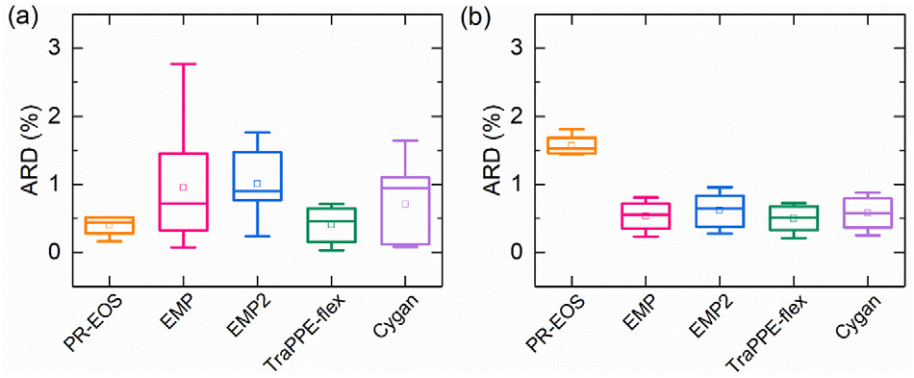

Fig. 5. ARDs of the calculated heat capacities for CO_2 by MD simulations with different force field models and PR-EOS. (a) isobaric heat capacity; (b) isochoric heat capacity.

value of the SPC/Fw model has the smallest deviation with an AARD of 2.07%. The AARD of isobaric heat capacity predicted by PR-EOS is 5.55%, which is close to that predicted by the TIP4P model. However, the prediction of PR-EOS for isochoric heat capacity is worse than that of the TIP4P model; the AARD for PR-EOS is 11.33% while that for TIP4P model is 3.4%, and the accuracy of PR-EOS increases with the increase of temperature. Moreover, the performance of PR-EOS is poor in near-critical region, for example, the ARDs of C_P and C_V is respectively 18.04% and 30.44% at temperature of 700 K.

Among the force field models for pure H_2O examined in this work, the TIP4P model exhibit the best accuracy. The same conclusion was also reached in the study by Jedlovszky et al. [50]; in the supercritical region of water, the TIP4P model in the two selected non-polarization models provides the best prediction of heat capacity. The conclusion of Kalinichev et al. [51] also verified that the prediction of the isobaric heat capacity of supercritical water using the TIP4P model is in good agreement with the experimental data. Given the preceding results of the simulations, the TIP4P model is recommended for water molecules in the simulation of mixtures.

The thermodynamic properties C_P, C_V, α, and κ_T of pure CO_2 are then calculated via MD simulations and compared to the results obtained by PR-EOS. In this study, four common force fields are tested, namely EPM, EPM2, Cygan, and TraPPE-flex. The results of MD simulation and PR-EOS calculation are presented in Fig. 4. All models exhibited improved accuracy with the increase of temperature, and are in good agreement with the values of the NIST data. The ARDs are shown in Fig. 5. The TraPPE-flex model performed the best; the AARDs of isobaric and isochoric heat capacity are 0.40% and 0.50%, respectively. The Cygan model performed the second best, with AARDs of 0.71% and 0.58%. The EPM and EPM2 models are slightly less accurate than the other models. The isobaric heat capacity calculated by PR-EOS has close accuracy compared to the MD simulations with the TraPPE-flex model, but the calculated isochoric heat capacity is worse than that obtained by the MD simulations; the AARD is 1.57%. According to the preceding simulation results, the TraPPE-flex model was selected for carbon dioxide molecules when predicting the heat capacity of mixtures.

3.2. Combining rules

Before the simulation of mixtures, the intermolecular parameters σ_{ij} and ε_{ij} should be defined from those of the pure compounds through a set of combining rules. Three common combining rules are tested in this work, namely the LB, Kong, and WH rules, as they do not require any additional parameters. The results of the simulation for H_2O/CO_2 mixtures ($x_{CO_2} = 40\%$) at a pressure of 25 MPa are shown in Fig. 6. The effect of the calculated isobaric and isochoric heat capacities using different combining rules is marginal. In addition, the Lorentz–Berthelot combining rule is most widely used, and is relatively simple for the determination of unlike LJ parameters. Therefore, the LB combining rules is recommended to determine the LJ parameters of unlike atoms of mixtures.

3.3. H_2O/CO_2 binary mixtures

The heat capacity and relevant thermodynamic properties of H_2O/CO_2 binary mixtures are calculated using MD simulations and PR-EOS

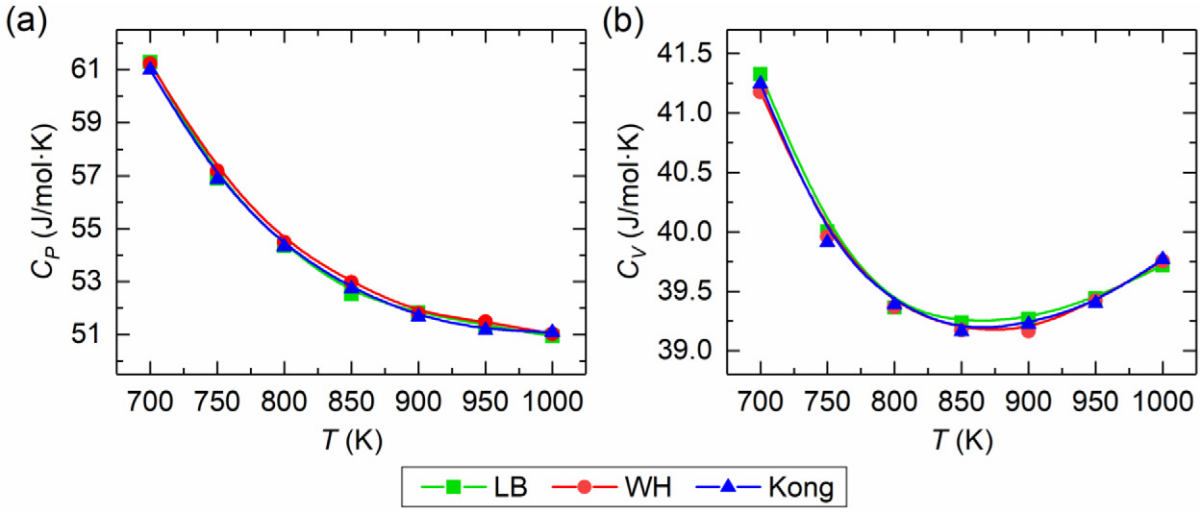

Fig. 6. Heat capacities calculated by MD simulation for H_2O/CO_2 mixtures ($x_{CO_2} = 40\%$) using different combining rules. (a) isobaric heat capacity; (b) isochoric heat capacity.

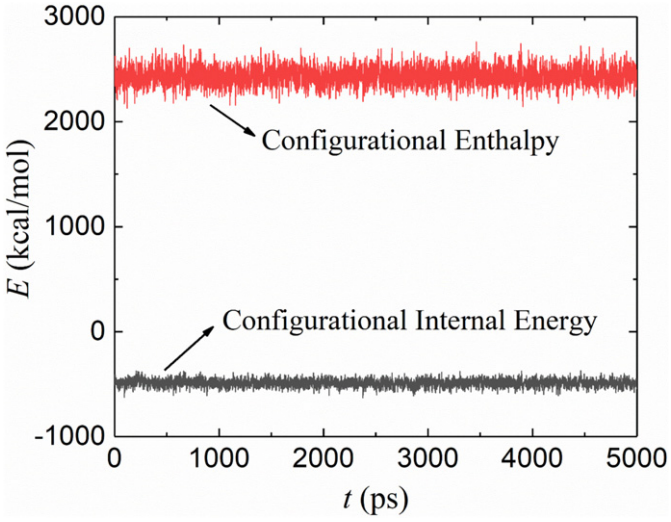

Fig. 7. Energy fluctuation of a simulation system for the H_2O/CO_2 mixture ($x_{CO_2} = 40\%$, $T = 850$ K).

calculations. The TIP4P and TraPPE-flex models are chosen for the simulation of H_2O/CO_2 mixtures due to their superior performance in the preceding simulations for pure H_2O and CO_2. Fig. 7 presents an example of the energy fluctuation of the system during the last 5 ns at 850 K when the mole fraction of CO_2 is 40%. Fig. 8 shows the results of simulations and PR-EOS under a pressure of 25 MPa and at temperatures between 700 and 1000 K when $x_{CO_2} = 10\%$, 20%, 30%, and 40%. The corresponding NIST data are also listed in the figure for comparison. It can be observed that the MD simulations generally overestimate the isobaric and isochoric heat capacities, except for one isobaric heat capacity estimation when the mole fraction of CO_2 is 10% at a temperature of 700 K. Both methods exhibit improved accuracy as the temperature increases. The AARDs of the calculated volume expansivity and isothermal compressibility for the MD simulations are respectively 3.62% and 3.20%, while they are 1.03% and 1.27% for PR-EOS.

Table 4
ARDs of heat capacities of H_2O/CO_2 mixtures calculated through MD Simulations.

T (K)	ARD (%)							
	$x_{CO2} = 10\%$		$x_{CO2} = 20\%$		$x_{CO2} = 30\%$		$x_{CO2} = 40\%$	
	C_P	C_V	C_P	C_V	C_P	C_V	C_P	C_V
700	3.704	7.476	3.405	9.760	5.559	9.249	5.177	8.213
750	3.080	6.322	3.750	7.170	4.757	6.872	3.757	5.514
800	2.870	5.505	3.427	5.519	3.039	4.873	2.723	3.720
850	4.792	4.260	3.533	4.004	2.145	3.165	1.318	2.771
900	2.528	3.189	2.516	2.977	1.372	2.450	1.390	1.993
950	1.871	2.502	2.047	2.266	1.591	1.793	1.081	1.416
1000	2.311	1.892	0.577	1.705	1.261	1.337	0.438	1.012
AARD	3.022	4.450	2.751	4.772	2.818	4.249	2.269	3.520

Table 4 exhibits the ARD between the results of the MD simulations and the NIST data. The AARDs of isobaric and isochoric heat capacities obtained by MD simulation are 2.72% and 4.25%, respectively. Table 5 lists the ARD of PR-EOS calculations, and it can be seen that the deviation of isochoric heat capacity decreases with the increase of the mole fraction of CO_2 due to the poor performance of PR-EOS for pure H_2O. The AARDs of isobaric and isochoric heat capacities obtained by PR-EOS are 2.02% and 2.99%, respectively. Thus, both the MD simulations and PR-EOS present good prediction accuracy, and the heat capacities predicted by PR-EOS are slightly more accurate than those obtained by MD simulations. However, the performance of PR-EOS is much poorer than that of the MD simulations when x_{CO_2} is relatively small and the

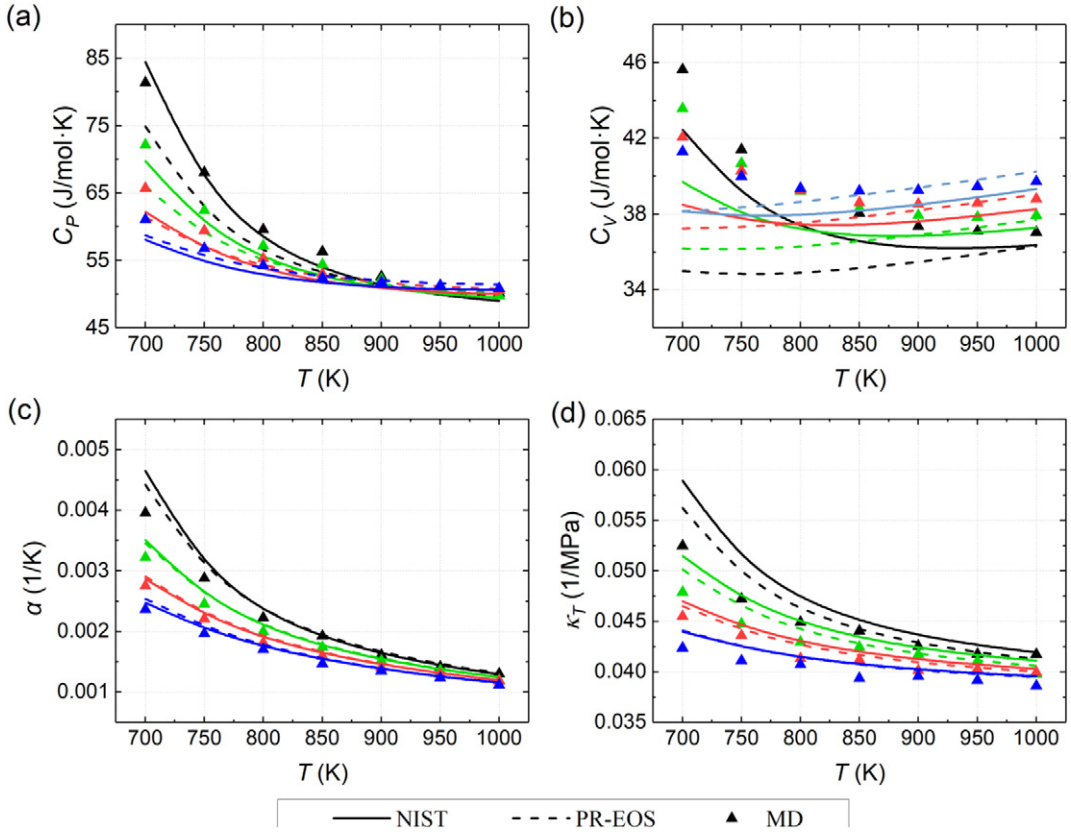

Fig. 8. Thermophysical properties as a function of temperature calculated by MD simulation and PR-EOS compared with NIST data for H_2O/CO_2 mixtures. (a) isobaric heat capacity; (b) isochoric heat capacity; (c) volume expansivity; (d) isothermal compressibility;

Table 5
ARDs of heat capacities of H_2O/CO_2 mixtures calculated through PR-EOS.

T (K)	ARD (%)							
	x_{CO2} = 10%		x_{CO2} = 20%		x_{CO2} = 30%		x_{CO2} = 40%	
	C_P	C_V	C_P	C_V	C_P	C_V	C_P	C_V
700	11.329	17.555	5.336	8.836	1.249	3.279	1.118	0.012
750	6.298	10.624	2.531	4.794	0.089	1.023	1.582	1.173
800	3.073	6.371	0.732	2.316	0.922	0.329	1.823	1.838
850	1.109	3.707	0.348	0.779	1.380	1.133	1.892	2.192
900	0.068	1.997	0.965	0.183	1.593	1.599	1.850	2.357
950	0.762	0.883	1.293	0.781	1.650	1.853	1.735	2.403
1000	1.154	0.146	1.438	1.148	1.607	1.972	1.580	2.374
AARD	3.399	5.898	1.806	2.691	1.213	1.598	1.654	1.764

temperature is below 800 K. For example, when the CO_2 mole fraction is only 10% at 700 K, the ARDs of isobaric and isochoric heat capacities obtained by MD simulation are 3.70% and 7.48%, respectively, but those of PR-EOS are 11.33% and 17.56%, respectively. It is obvious that the MD simulation is much better than PR-EOS near the critical temperature of water, and this may be due to the effect of the hydrogen bonds of water.

Fig. 9 illustrates the four thermodynamic properties with different mole fractions of CO_2 at a pressure of 25 MPa and temperature of 850 K. The accuracy of both MD simulations and PR-EOS is improved as the mole fraction of CO_2 increases. The AARDs of the isobaric and isochoric heat capacities, volume expansivity, and isothermal compressibility obtained by MD are 1.96%, 2.18%, 2.88% and 1.76%, respectively, while those predicted by PR-EOS are 1.18%, 2.59%, 1.86%, and 0.88%, respectively. These results demonstrate that MD simulations and PR-EOS are both well able to predict these thermodynamic properties.

3.4. Structural analysis

The radial distribution function (RDF) is a physical quantity that reflects the microstructural characteristics of a fluid in terms of its structure and the sizes of clusters. Fig. 10 presents RDFs for H_2O/CO_2 mixtures in MD simulations at 25 MPa and temperatures between 700 and 1000 K with a CO_2 mole fraction of 10%. Fig. 10(a) depicts the total RDF ($g(r)_{total}$), which is the weighted sum of $g(r)$ for all the different atom pairs. A single peak is observed at the nearest-neighbor distance of about 3.3 Å; it then disappears gradually, and the system tends to the ideal gas state. $g(r)_{O(H_2O)-H(H_2O)}$ describes the O—H distance for neighboring H_2O molecules. As shown in Fig. 10(b), the first peak (or shoulder) appears and is located at about 2.0 Å due to the H-bond. It can be inferred that the effect of the H-bond is relatively large around a temperature of 700 K, and weakens with the increase of temperature. All RDFs show that the peak decreases with the increase of temperature in a supercritical condition, i.e., the sizes of small clusters and the average number of H-bonds per molecule decrease with the increase of temperature. Moreover, Fig. 11 shows the average H-bond number n_{OH} as a function of temperature for both pure water and H_2O/CO_2 mixtures at different x_{CO_2}. Here the values of n_{OH} calculated for pure water are not exactly agree with those in Ref. [6], and the difference is coming from the different force field models employed. It can be seen that the H-bond effect is weakened more and more with increasing CO_2 content for the H_2O/CO_2 mixtures, and this can explain why PR-EOS can achieve good accuracy at higher mole fractions of CO_2 in near-critical regions of water. In fact, MD simulations have the advantage over PR-EOS that can describe the effects of H-bonds. As reported by Silverstein et al. [52], for water, the heat capacity actually describes the extent to which H bonds are broken with increasing temperature. This should be the reason that the MD method exhibits better

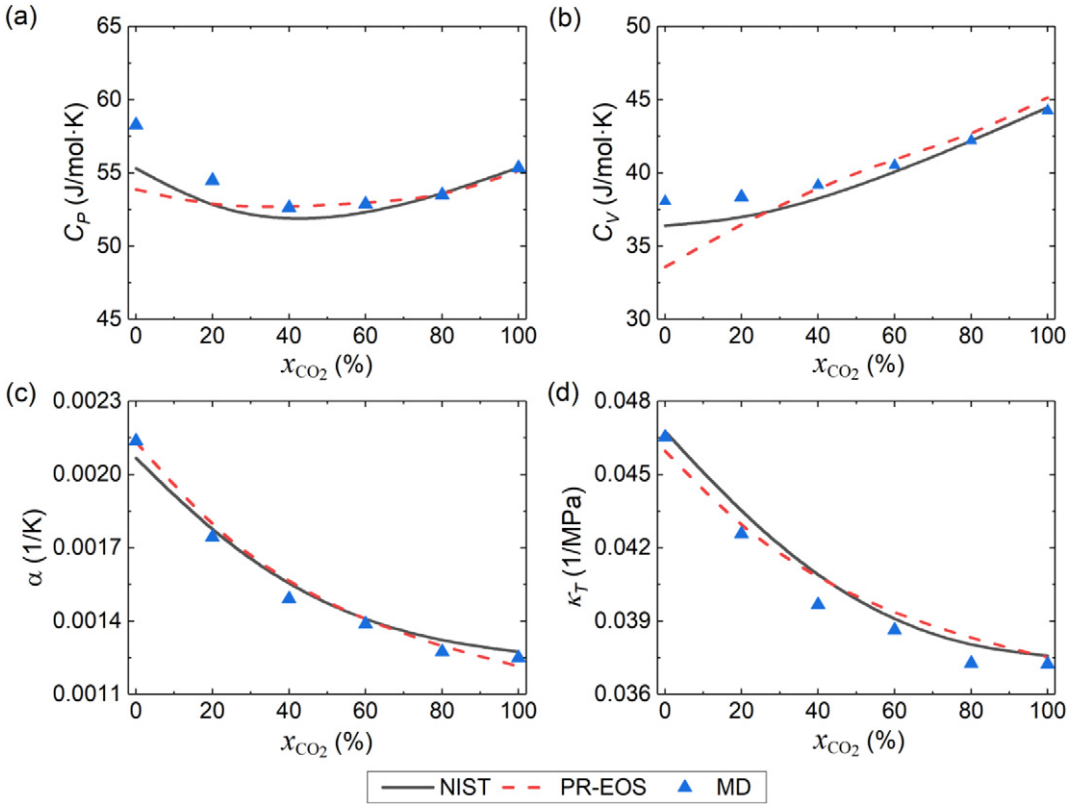

Fig. 9. Thermophysical properties as a function of x_{CO_2} calculated by MD simulation and PR-EOS compared with NIST data for H_2O/CO_2 mixtures. (a) isobaric heat capacity; (b) isochoric heat capacity; (c) volume expansivity; (d) isothermal compressibility; (T = 850 K).

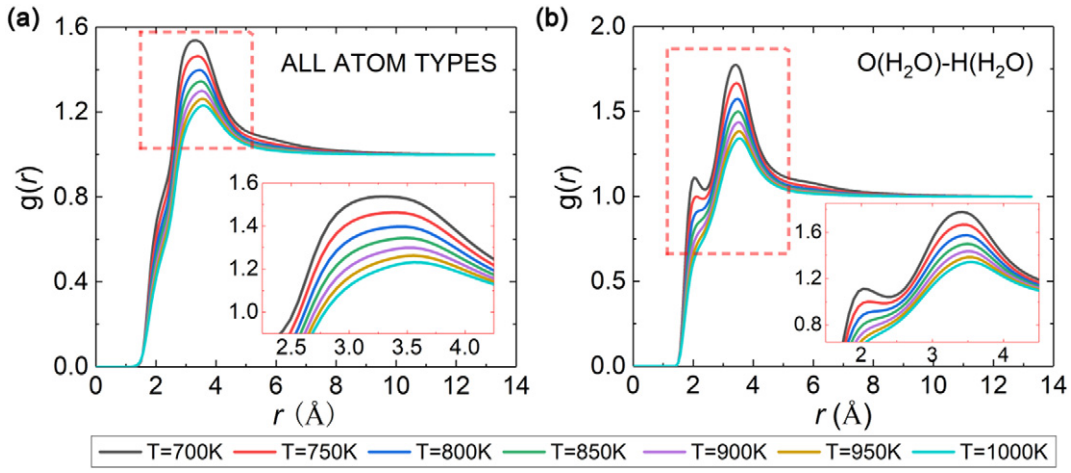

Fig. 10. RDF between different atom types for H_2O/CO_2 mixtures: (a) RDF for all atom types; (b) RDF for O(H_2O)-H(H_2O); (x_{CO_2}=10%).

performance in the prediction of heat capacity of both pure H_2O and H_2O/CO_2 mixtures at higher mole fractions of H_2O in near-critical regions of water.

4. Conclusion

The isobaric and isochoric heat capacities, as well as the volume expansivity and isothermal compression, of pure working fluid H_2O and CO_2 and H_2O/CO_2 binary mixtures in the supercritical region are investigated by using MD simulations and PR-EOS. The comparisons show that the TIP4P model and TraPPE-flex model are respectively optimal for the simulation of the heat capacity of supercritical H_2O and CO_2 pure fluid. Using NIST data as a reference, it is found that both MD simulations and PR-EOS generally exhibit comparable and acceptable performance in prediction of the heat capacities of the supercritical fluids. However, in near-critical region for pure supercritical H_2O and the supercritical H_2O/CO_2 mixtures at higher mole fractions of H_2O, PR-EOS exhibit poor prediction accuracy while MD simulation models achieve much better performance. This work is helpful for guiding the future investigation of the heat capacity of other working mixtures, e.g., $H_2O/H_2/CO_2$ mixtures and $H_2O/H_2/CO_2/CH_4$ mixtures, in the thermodynamic systems based on the supercritical water gasification of coal.

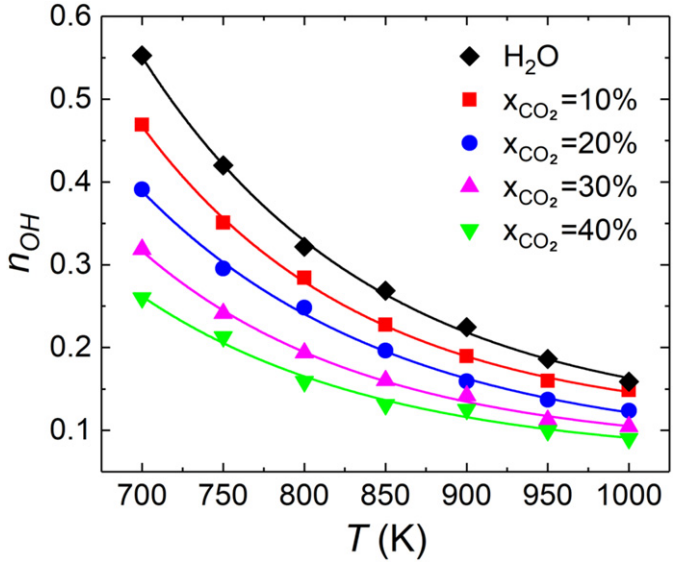

Fig. 11. The average H-bond number n_{OH} as a function of temperature for both pure water and H_2O/CO_2 mixtures at different x_{CO_2}.

Declaration of competing interest

The authors declare no competing financial interest.

Acknowledgments

This work was supported by the National Key Research and Development Program of China (Grant No. 2016YFB0600100) and the Natural Science Foundation of Hebei Province of China (Grant No. E2019502138).

References

[1] L. Guo, H. Jin, Y. Lu, Supercritical water gasification research and development in China, J. Supercrit. Fluids 96 (2015) 144–150.
[2] L. Guo, H. Jin, Z. Ge, Y. Lu, C. Cao, Industrialization prospects for hydrogen production by coal gasification in supercritical water and novel thermodynamic cycle power generation system with no pollution emission, Sci. China Technol. Sci. 58 (2015) 1989–2002.
[3] J. Xu, E. Sun, M. Li, H. Liu, B. Zhu, Key issues and solution strategies for supercritical carbon dioxide coal fired power plant, Energy 157 (2018) 227–246.
[4] E. Sun, J. Xu, H. Hu, B. Zhu, J. Xie, Y. Zheng, Analysis of a coal-fired power system integrated with a reheat S-CO_2 cycle, Energy Procedia 158 (2019) 1461–1466.
[5] Y. Le Moullec, Conceptual study of a high efficiency coal-fired power plant with CO_2 capture using a supercritical CO_2 Brayton cycle, Energy 49 (2013) 32–46.
[6] X. Yang, Y. Feng, J. Xu, J. Jin, Y. Liu, B. Cao, Numerical study on transport properties of the working mixtures for coal supercritical water gasification based power generation systems, Appl. Therm. Eng. 114228 (2019).
[7] X. Yang, C. Duan, J. Xu, Y. Liu, B. Cao, A numerical study on the thermal conductivity of $H_2O/CO_2/H_2$ mixtures in supercritical regions of water for coal supercritical water gasification system, Int. J. Heat Mass Transf. 135 (2019) 413–424.
[8] X. Yang, J. Xu, S. Wu, M. Yu, B. Hu, B. Cao, J. Li, A molecular dynamics simulation study of PVT properties for $H_2O/H_2/CO_2$ mixtures in near-critical and supercritical regions of water, Int. J. Hydrog. Energy 43 (2018) 10980–10990.
[9] S. Cheng, F. Shang, W. Ma, H. Jin, N. Sakoda, X. Zhang, L. Guo, Density data of two (H_2+CO_2) mixtures and a (H_2+CO_2+CH_4) mixture by a modified Burnett method at temperature 673 K and pressures up to 25 MPa, J. Chem. Eng. Data 64 (2019) 1693–1704.
[10] Y. Liu, W. Hong, B. Cao, Machine learning for predicting thermodynamic properties of pure fluids and their mixtures, Energy 116091 (2019).
[11] H. Krienke, G. Schmeer, A. Straßer, Thermodynamic properties of water from combined quantum and statistical mechanics in the temperature range from 273.16 to 423.15 K, J. Mol. Liq. 113 (2004) 115–124.
[12] S. Krishtal, M. Kiselev, Y. Puhovski, T. Kerdcharoen, S. Hannongbua, K. Heinzinger, Study of the hydrogen bond network in sub-and supercritical water by molecular dynamics simulations, Z. Naturforsch. A 56 (2001) 579–584.
[13] A. Saul, W. Wagner, A fundamental equation for water covering the range from the melting line to 1273 K at pressures up to 25000 MPa, J. Phys. Chem. Ref. Data 18 (1989) 1537–1564.
[14] W. Wagner, A. Pruß, The IAPWS formulation 1995 for the thermodynamic properties of ordinary water substance for general and scientific use, J. Phys. Chem. Ref. Data 31 (2002) 387–535.
[15] R. Span, W. Wagner, A new equation of state for carbon dioxide covering the fluid region from the triplepoint temperature to 1100K at pressures up to 800MPa, J. Phys. Chem. Ref. Data 25 (1996) 1509–1596.
[16] G. Ernst, U.E. Hochberg, Flow-calorimetric results for the specific heat capacity cp of CO_2, of C_2H_6, and of (0.5CO_2+0.5C_2H_6) at high pressures, J. Chem. Thermodyn. 21 (1989) 407–414.

[17] M.P.E. Ishmael, M.Z. Lukawski, J.W. Tester, Isobaric heat capacity (Cp) measurements of supercritical fluids using flow calorimetry: equipment design and experimental validation with carbon dioxide, methanol, and carbon dioxide-methanol mixtures, J. Supercrit. Fluids 117 (2016) 72–79.
[18] C. Avendano, T. Lafitte, A. Galindo, SAFT-γ force field for the simulation of molecular fluids. 1. A single-site coarse grained model of carbon dioxide, J. Phys. Chem. B 115 (2011) 11154–11169.
[19] P. Ungerer, C. Nieto-Draghi, B. Rousseau, G. Ahunbay,V, Lachet, Molecular simulation of the thermophysical properties of fluids: from understanding toward quantitative predictions, J. Mol. Liq. 134 (2007) 71–89.
[20] R.K. Endo, Y. Fujihara, M. Susa, Calculation of the density and heat capacity of silicon by molecular dynamics simulation, High Temp.–High Pressures 35 (2003) 505–511.
[21] J. Nichele, A.B. de Oliveira, L.S. de B. Alves, I. Borges Jr, Accurate calculation of near-critical heat capacities C_P and C_V of argon using molecular dynamics, J. Mol. Liq. 237 (2017) 65–70.
[22] J. Nichele, C.R.A. Abreu, L.S. de B. Alves, I. Borges Jr., Accurate non-asymptotic thermodynamic properties of near-critical N_2 and O_2 computed from molecular dynamics simulations, J. Supercrit. Fluids 135 (2018) 225–233.
[23] I. Shvab, R.J. Sadus, Thermophysical properties of supercritical water and bond flexibility, Phys. Rev. E 92 (2015), 012124.
[24] M.P.E. Ishmael, L.B. Stutzman, M.Z. Lukawski, F.A. Escobedo, J.W. Tester, Heat capacities of supercritical fluid mixtures: comparing experimental measurements with Monte Carlo molecular simulations for carbon dioxide-methanol mixtures, J. Supercrit. Fluids 123 (2017) 40–49.
[25] M.H. Ghatee, H. Karimi, K. Shekoohi, Structural, mechanical and thermodynamical properties of silver amalgam filler: a Monte Carlo simulation study, J. Mol. Liq. 211 (2015) 96–104.
[26] A. Congiunti, C. Bruno, E. Giacomazzi, Supercritical combustion properties, in: 41st Aerospace Sciences Meeting and Exhibition, (2003) 478.
[27] K. Nasrifar, Comparative study of eleven equations of state in predicting the thermodynamic properties of hydrogen, Int. J. Hydrog. Energy 35 (2010) 3802–3811.
[28] K. Nasrifar, O. Bolland, Prediction of thermodynamic properties of natural gas mixtures using 10 equations of state including a new cubic two-constant equation of state, J. Pet. Sci. Eng. 51 (2006) 253–266.
[29] E.W. Lemmon, M.L. Huber, M.O. McLinden, NIST Standard Reference Database 23, Reference fluid thermodynamic and transport properties-REFPROP, Version 9, 1, National Institute of Standards and Technology, Standard Reference Data Program, 2013.
[30] H.J.C. Berendsen, J.P.M. Postma, W.F. van Gunsteren, J. Hermans, Interaction Models for Water in Relation to Protein Hydration, Intermolecular Forces, Springer, Dordrecht, 1981 331–342.
[31] H.J.C. Berendsen, J.R. Grigera, T.P. Straatsma, The missing term in effective pair potentials, J. Phys. Chem. 91 (1987) 6269–6271.
[32] Y. Wu, H.L. Tepper, G.A. Voth, Flexible simple point-charge water model with improved liquid-state properties, J. Chem. Phys. 124 (2006), 024503.
[33] W.L. Jorgensen, J. Chandrasekhar, J.D. Madura, R.W. Impey, M.L. Klein, Comparison of simple potential functions for simulating liquid water, J. Chem. Phys. 79 (1983) 926–935.
[34] D.J. Price, C.L. Brooks III, A modified TIP3P water potential for simulation with Ewald summation, J. Chem. Phys. 121 (2004) 10096–10103.
[35] J.L.F. Abascal, C. Vega, A general purpose model for the condensed phases of water: TIP4P/2005, J. Chem. Phys. 123 (2005), 234505.
[36] J.G. Harris, K.H. Yung, Carbon dioxide's liquid-vapor coexistence curve and critical properties as predicted by a simple molecular model, J. Phys. Chem. 99 (1995) 12021–12024.
[37] R.T. Cygan, V.N. Romanov, E.M. Myshakin, Molecular simulation of carbon dioxide capture by montmorillonite using an accurate and flexible force field, J. Phys. Chem. C 116 (2012) 13079–13091.
[38] M.E. Perez-Blanco, E.J. Maginn, Molecular dynamics simulations of CO_2 at an ionic liquid interface: adsorption, ordering, and interfacial crossing, J. Phys. Chem. B 114 (2010) 11827–11837.
[39] H.A. Lorentz, Ueber die Anwendung des Satzes vom Virial in der kinetischen Theorie der Gase, Ann. Phys. 248 (1881) 127–136.
[40] D. Berthelot, Sur le mélange des gaz, C. R. Acad. Sci. Paris 126 (1898) 1703–1706.
[41] M. Waldman, A.T. Hagler, New combining rules for rare gas van der Waals parameters, J. Comput. Chem. 14 (1993) 1077–1084.
[42] C.L. Kong, Combining rules for intermolecular potential parameters. II. Rules for the Lennard-Jones (12–6) potential and the Morse potential, J. Chem. Phys. 59 (1973) 2464–2467.
[43] M.P. Allen, D.J. Tildesley, Computer Simulation of Liquids, Oxford University Press, Oxford, 1987.
[44] D.W. Green, R.H. Perry, Perry's Chemical Engineers' Handbook, 8th ed. McGraw Hill Professional, New York, 2007.
[45] D.Y. Peng, D.B. Robinson, A new two-constant equation of state, Ind. Eng. Chem. Fundam. 15 (1) (1976) 59–64.
[46] T.Y. Kwak, G.A. Mansoori, Van der Waals mixing rules for cubic equations of state. Applications for supercritical fluid extraction modelling, Chem. Eng. Sci. 41 (1986) 1303–1309.
[47] B.E. Poling, J.M. Prausnitz, J.P. O'Connell, the Properties of Gases and Liquids, McGraw-Hill, New York, 2001.
[48] S. Plimpton, Fast parallel algorithms for short-range molecular dynamics, J. Comput. Phys. 117 (1995) 1–19.
[49] L. Verlet, Computer experiments on classical fluids. I. Thermodynamical properties of Lennard-Jones molecules, Phys. Rev. 159 (1967) 98.
[50] P. Jedlovszky, J. Richardi, Comparison of different water models from ambient to supercritical conditions: a Monte Carlo simulation and molecular Ornstein–Zernike study, J. Chem. Phys. 110 (1999) 8019–8031.
[51] A.G. Kalinichev, Monte Carlo simulations of water under supercritical conditions, I. Thermodynamic and Structural, Z. Naturforsch. A 46 (1991) 433–444.
[52] K.A.T. Silverstein, A.D.J. Haymet, K.A. Dill, A simple model of water and the hydrophobic effect, J. Am. Chem. Soc. 120 (1998) 3166–3175.